Materials Science & Engineering A 812 (2021) 141137

Contents lists available at ScienceDirect

Materials Science & Engineering A

journal homepage: http://www.elsevier.com/locate/msea

Coarsening of Laves phase and creep behaviour of a Re-containing 10% Cr-3% Co-3% W steel

A. Fedoseeva *, I. Nikitin, N. Dudova, R. Kaibyshev

Belgorod National Research University, Pobeda 85, Belgorod, 308015, Russia

ARTICLE INFO

Keywords:
Steel
Electron microscopy
Creep
Diffusion
Precipitation
Laves phase
Coarsening

ABSTRACT

The coarsening of Laves phase in a Re-containing 10% Cr-3% Co-3% W steel during both creep and ageing at 923 K was investigated. The depletion of W solutes from the ferrite matrix is accompanied with the precipitation of Laves phase, wherein creep strain accelerates both these processes. The equilibrium W content in the ferritic matrix of 1.24 wt% and the volume fraction of Laves phase of 1.6% is reached after 500 h of creep and 1000 h of ageing. This is related to lower activation energy for W diffusion upon creep testing. The coarsening of Laves phase obeys Ostwald ripening and can be described in terms of Lifshitz-Slyozov-Wagner theory: $d^4 - d_0^4 = K_p(t\text{-}t_0)$, where $K_p = 3.70\text{–}3.80 \times 10^{-11}$ μm^4 s^{-1} for both creep and ageing suggesting that the coarsening of these particles should be controlled by grain boundary diffusion. No strain-induced coarsening of Laves phase is observed. Growth of the Laves phase particles located on the lath boundaries and the high-angle boundaries of the blocks, packets and prior austenite grains occurs in independent manner. The Laves phase particles located on the high-angle boundaries are susceptible to coarsening that leads to appearance of the particles with dimensions >200 nm. The Laves phase particles located on the lath boundaries dissolve with a low rate. Dense chains of Laves phase on the lath boundaries retain up to high creep time giving a significant contribution to creep behaviour.

1. Introduction

Creep resistant 9–12% Cr martensitic steels are widely used as materials for fossil power plants working at temperatures up to 893 K [1–3]. The high creep resistance of the 9–12% Cr steels is attributed to complex microstructural design provided by superposition of solid solution hardening, dispersion strengthening, (sub)structural strengthening and dislocation strengthening [1,3,4]. Normalizing followed by tempering produces the tempered martensite lath structure (TMLS) composed of a hierarchical sequence of structural elements, i.e. prior austenite grains (PAG), packets, blocks, and laths with a high density of free dislocations. M(C,N) carbonitrides and $M_{23}C_6$ carbides precipitate in the ferritic matrix and on the boundaries, respectively [1,2,4,5]. (Sub)structural strengthening is provided by laths and blocks, while dislocation strengthening is associated with a high density of lattice dislocations [1,4,5]. M(C,N) carbonitrides and $M_{23}C_6$ carbides provide dispersion strengthening; alloying elements such as chromium, cobalt, tungsten, molybdenum, rhenium contribute to solid solution strengthening [1,4,6–9].

Superior creep strength is attributed to stability of the TMLS. Knitting reactions between lattice dislocations and lath boundaries lead to loss of stability of the TMLS due to the transformation of the dislocation lath boundaries to subgrain ones [1,9–15]. Substitutional alloying elements, matrix dispersoids and boundary particles slow down these knitting reactions [1,9–15]. In addition, the boundary $M_{23}C_6$ carbides and Laves phase particles precipitated during tempering and creep effectively pin the (sub)boundaries by exerting a high Zener drag pressure that restricts mobility of the (sub)boundaries evolved from the lath boundaries [7,11,12,16–20]. The main disadvantage of the high-Cr martensitic steels is degradation in the long-term creep strength that results in the progressive decrease in allowable stress with increasing service period [1,9–14]. This degradation is described in terms of the creep strength breakdown and is attributed to strain-induced coarsening of secondary phase particles and/or depletion of tungsten and molybdenum from solid solution followed by the transformation of the TMLS into the subgrain structure [1,9–14]. It was shown [1,3,9–12,16–20] that stability of M(C,N) carbonitrides and a reduction of coarsening rate of boundary $M_{23}C_6$ carbides under creep conditions is a key issue for superior long-term creep strength of the high-Cr martensitic steels [3,7,15,16]. Strain-induced coarsening of $M_{23}C_6$ carbides and replacement of

* Corresponding author.
E-mail address: fedoseeva@bsu.edu.ru (A. Fedoseeva).

https://doi.org/10.1016/j.msea.2021.141137
Received 3 July 2020; Received in revised form 16 March 2021; Accepted 16 March 2021
Available online 23 March 2021

the nanoscale M(C,N) carbonitrides by the coarse Z-phase (Cr,V)N particles are responsible for instability of the TMLS under creep conditions [1,3,9–14,16–21]. Precipitate design based on the addition of boron to approximately 0.01 wt% and decreasing the N content to lowest possible value was suggested by the National Institute for Materials Science (NIMS) to suppress/hinder strain-induced coarsening of M(C,N) carbonitrides and $M_{23}C_6$ carbides [1,9,22–24]. The creep strength of these steels is controlled by coarsening of $M_{23}C_6$ carbides located on the lath boundaries, since the dispersion of M(C,N) carbonitrides retains virtually unchanged after creep [12,16,25,26].

A Re-containing 10% Cr-3% Co-3% W steel with the low N content of 0.002 wt% and the high B content of 0.008 wt% exhibiting creep rupture time of about 11,000 h at 923 K and 140 MPa was developed in accordance with this alloying philosophy [26,27]. As shown in the previous research [26], this steel demonstrates a unique short-term creep behaviour (Fig. 1), which is characterized by high and low absolute values of $d\ln\dot{\varepsilon}/d\varepsilon$ associated with the reaction-rate kinetics controlled by rearrangement of dislocations during the transient and tertiary creep stages, respectively [1–12,25,26,28–30]. The $d\ln\dot{\varepsilon}/d\varepsilon$ value of −445 is

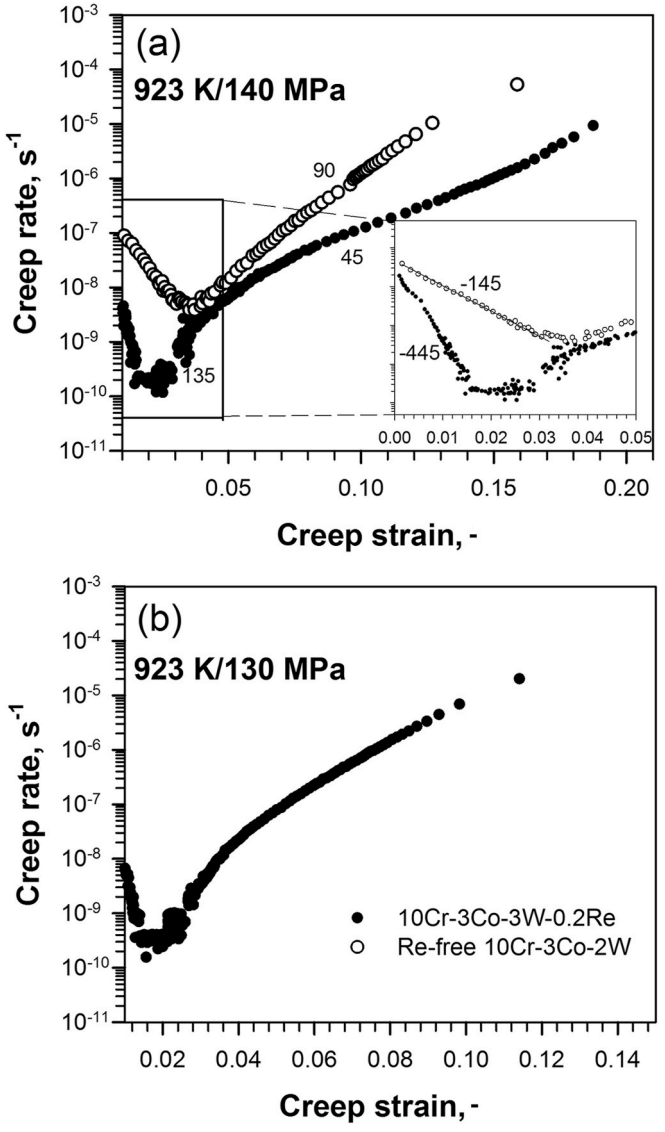

Fig. 1. Creep rate vs. strain curves of the 10% Cr-3% Co-3% W-0.2% Re steel [26] (a,b) and Re-free 10% Cr-3% Co-2% W steel [10] (a) with low N and high B contents at an applied stress of 140 (a) and 130 (b) MPa. Numbers in (a) indicate the slopes of the curves in the transient and tertiary creep stages ($d\ln\dot{\varepsilon}/d\varepsilon$) estimated using the method suggested in Ref. [30].

attributed to the precipitation of Laves phase on the lath boundaries during transient creep stage [11,12,26,31]. The formation of the dense chains of $M_{23}C_6$ and M_6C carbides and Laves phase increases the number of obstacles for the dislocation glide along the laths due to attractive interaction between gliding dislocations and these particles that increases the value of dispersion strengthening [4,6–8,12,26,31]. This interaction restricts ability of gliding dislocations to rearrangement by climb that slows down the knitting reaction that expands the range of short-term creep to 10,000 h and decreases the minimum creep rate, $\dot{\varepsilon}_{min}$, to a very low value of 2×10^{-10} s^{-1} [7,11,12,16,26]. The expansion of short-term region to higher rupture times is caused by decreased rate of the particle coarsening owing to Re additives [26].

The Re-containing steel exhibits unusual two-stage tertiary creep behaviour [26]. The first stage of tertiary creep is characterized by a high $d\ln\dot{\varepsilon}/d\varepsilon$ value of 135 and a low $d\ln\dot{\varepsilon}/d\varepsilon$ value of 45 was observed at the second stage of tertiary creep (Fig. 1) [26]. Therefore, the kinetic reactions [28,29] occur with a high rate after termination of the minimum creep rate and are slowed down with increasing creep strain more than 5% (Fig. 1) [26]. This tertiary creep behaviour is not observed in the high-Cr steel with the high boron content [10,12,16,25] and takes place in a 9% Cr-3% Co-3% W-0.6% Mo steel with the low boron content [11]. Origin of this tertiary creep behaviour remains unknown [11]. The transformation of minor portion of the TMLS into the subgrain structure is found after rupture [26]. The chains of the boundary particles on the lath boundaries retain; the TMLS is in dominance [26]. The role of particles precipitated on the lath boundaries in microstructural design of new generation of the high-Cr steels with the increased boron content will be established on the base of experimental data presented in this work.

The previous studies [26,27] were focused on the effect of Re on the short-term creep properties of the 10% Cr–3% Co steel with the low N and high B contents by comparison of Re-containing and Re-free steels. As shown in Refs. [26,27], Re didn't provide the improved solid solution strengthening and didn't affect the kinetic of W depletion from ferritic matrix, whereas Re slowed down the coarsening of $M_{23}C_6$ carbides and Laves phase located at the low-angle boundaries. This indicates that Laves phase may also prevent the migration of the lath boundaries during creep for long time like $M_{23}C_6$ carbides. To understand the reasons of superior short-term creep resistance of Re-containing 10% Cr-3% Co-3% W steel [26], the behaviour of Laves phase (the nucleation and coarsening) should be paid the additional attention. The Laves phase nucleation through W-rich carbide (M_6C) was considered in the companion article [31] in detail. The aim of the present study is to consider the coarsening behaviour of Laves phase in the Re-containing 10% Cr-3% Co-3% W steel exhibiting unusual creep behaviour.

2. Experimental

A Re-containing 10% Cr-3% Co-3% W steel with the chemical composition of (in wt%) Fe (bal.)–0.11C–9.85Cr–3.20Co–2.86W-0.13Mo–0.22Cu-0.03Si–0.14Mn–0.03Ni-0.23V–0.07Nb–0.002N–0.008B-0.17Re was prepared by vacuum induction melting as 100 kg ingots. The actual chemical compositions of the steel was determined using an optical emission spectrometer, FOUNDRY-MASTER UVR, a nitrogen, hydrogen and oxygen analyzer, METEK-300/600, and a scanning electron microscope, Nova NanoSEM, with an energy dispersive X-ray spectroscope. Square bars with an initial 11 mm × 11 mm cross-section were cast and hot forged. Next, this steel was solution treated at 1323 K for 1 h followed by normalizing and finally tempered at 1043 K for 3 h. Computer-controlled ATS Lever Arm Testers, model #2330, with WinCCS II Software (Applied Test Systems, Inc., Butler, PA) were used for the creep tests. Creep strain was measured using HEIDENHAIN length gauge (MT 1271) with accuracy ±0.2 μm. The 3-Zone high-temperature furnace was used. The temperature in the furnace was constantly monitored throughout the test by three thermocouples type K. The difference between the experimental

temperature and the nominal test temperature didn't exceed 2 K. The specimen was clamped with grips that were allowed to move only along the loading direction. Flat specimens with a gauge length of 25 mm and a cross section of 7 mm × 3 mm were crept at 923 K under the applied stresses of 130, 140, 160, 180 and 200 MPa until rupture. Under an applied stress of 130 MPa, the creep test was interrupted after achieving strains of 1% (254 h), 1.5% (3500 h) and 2% (5875 h) corresponding to the transient creep stage, steady-state creep stage and the first stage of tertiary creep (Fig. 1b, Table 1). The specimens corresponded to long-term ageing were taken from the grip portions of crept samples (Table 1). Additionally, long-term ageing at 923 K for 1000 h was carried out separately (Table 1). The structural characterizations attributed to creep and long-term ageing were carried out in the gauge and grip sections of crept samples, respectively, using a transmission electron microscope JEOL–2100 (TEM) with an INCA energy dispersive X-ray spectrometer (EDS) on the ruptured creep specimens. The TEM specimens were prepared by electropolishing at room temperature using a solution of 10 pct perchloric acid in glacial acetic acid with Struers « Tenupol-5» machine. The dislocation densities in the grain/subgrain interiors were estimated as a number of intersections of individual dislocations with upper/down foil surfaces per unit area on at least six arbitrarily selected typical TEM images for each data point. The precipitates were identified from both the chemical analysis and the selected-area diffraction method on at least 200 particles on the each portion by using extraction carbon replicas. The carbon replicas were prepared by using Q 150REQuorum vacuum deposition machine. The Nova NanoSEM and Quanta 600 FEG scanning electron microscopes (SEM) together with TEM were used for examination of Laves phase distribution. The Laves phase particles are clearly distinguished from $M_{23}C_6$ carbides by its bright contrast in the Z-contrast in SEM and chemical composition [32,33].

The number density, N_V, of Laves phase per unit volume was calculated using the equation:

$$N_V = \frac{N_T}{A_s(t + d_t)} \quad (1)$$

where N_T is the total number of precipitates, A_s is the area selected in the TEM/SEM image, t is the thickness of foil, d_t is diameter of particles. The foil thickness was determined by the convergent beam electron diffraction method based on Kossel-Möllenstedt fringe oscillations [34] and averaged using at least three measurements for each TEM image. The experimental volume fraction of Laves phase, f_V, was determined by multiplying the average particle volume and number density per unit volume:

$$f_V = \frac{N_V \pi d_t^2 t}{4} \quad (2)$$

The particle coarsening kinetic was calculated using Prisma-software on the base of Calphad Database Calculation with the kinetic MOBFE1 and the thermodynamic TCFE6 databases. The model compositions consisting of Fe, Cr, Mo, W and Co in accordance with the chemical composition of the steel studied were used for estimating the coarsening of the Laves phase particles assuming that a grain boundary is a nucleation site. The interfacial energy was estimated by the comparison of calculated kinetic of the particle growth using the Prisma-software and the experimental data [35].

3. Results

3.1. Tempered structure

The TMLS after tempering was described in the previous works [26,27] and the companion article [31] in detail. The structural parameters of the Re-containing steel in the tempered state are presented in Table 2. The mean size of martensitic laths was about 290 ± 30 nm; dislocation density was 2×10^{14} m^{-2}. Three types of the secondary particles were observed. Boundary $M_{23}C_6$ carbides with a mean size of 67 nm and W-rich M_6C (Fe_3W_3C) carbides with a mean size of 28 nm precipitated on low- (LAB) and high-angle boundaries (HAB) (Table 2) [31]. Nb(C,N) carbonitrides with a mean size of 37 nm determined the size of prior austenite grain size during austenitization (Table 2) [31]; PAG size was 59 μm [36].

3.2. Evolution of TMLS and a dispersion of secondary phase particles during long-term ageing

Figs. 2 and 3 show the microstructural evolution of the Re-containing 10% Cr-3% Co-3% W steel during long-term ageing; the structural parameters are summarized in Table 2. The TMLS retained after long-term ageing for about 11,000 h. The lath thickness, dimensions of M(C,N) carbonitrides and $M_{23}C_6$ carbides increased insignificantly (Table 2). The chains of $M_{23}C_6$ carbides on the lath boundaries retained up to 5875 h and tended to dissolve upon further ageing (Figs. 2 and 3). After long-term ageing for about 11,000 h, these chains were rarely observed on the lath boundaries, while the chains of $M_{23}C_6$ carbides retained on the block boundaries (Fig. 2d). Lattice dislocation density decreased by a factor of 2 after long-term ageing for about 11,000 h (Table 2). No evidence for transformation of the TMLS into the subgrain structure during long-term ageing for about 11,000 h at 923 K was revealed; the average size of the martensitic laths retained less than 500 nm even after about 11,000 h of ageing (Figs. 2 and 3, Table 2).

Table 2
Structural parameters of the 10% Cr-3% Co-3% W-0.2% Re steel in the tempered state and some aged states for different times at 923 K.

Ageing time, h	Lath size, nm	Subgrain size, nm	ρ_{disl}, × 10^{14} m^{-2}	The mean size of particles, nm			
				$M_{23}C_6$	Nb (C, N)	Laves phase	M_6C
tempering	293 ± 20	270 ± 20	1.98 ± 0,1	67 ± 7	37 ± 4	–	28 ± 2
440	348 ± 20	363 ± 20	1.37 ± 0,1	73 ± 10	45 ± 5	136 ± 20	90 ± 5
1000	360 ± 20	360 ± 20	1.20 ± 0.1	75 ± 10	45 ± 5	165 ± 20	–
3500	360 ± 20	350 ± 20	1.20 ± 0.1	75 ± 10	45 ± 5	155 ± 20	–
5875	350 ± 20	330 ± 20	1.10 ± 0.1	78 ± 10	45 ± 5	180 ± 20	–
10,987	350 ± 20	310 ± 20	1.04 ± 0.1	80 ± 10	45 ± 5	200 ± 20	–

Table 1
Creep and ageing time for tests (923 K) used in the present investigation.

Creep test conditions							
Nominal stress, MPa	200 Ruptured	180 Ruptured	130 Interrupted (1.5%)	160 Ruptured	130 Interrupted (1.5%)	130 Interrupted (2%)	140 Ruptured
Time, h	8	83	254	440	3500	5875	10,987
Long-term ageing conditions							
Time, h	8	83	254	440	1000	3500	5875	10,987

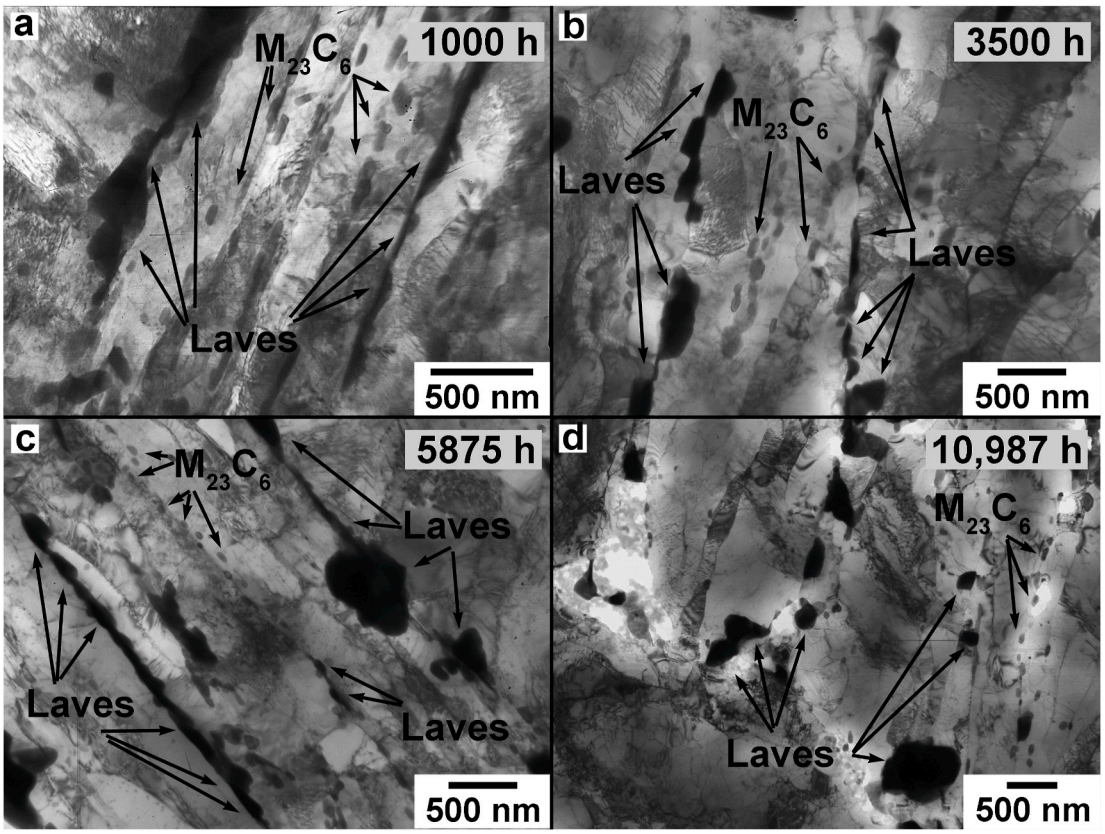

Fig. 2. TEM images of microstructure of the Re-containing steel studied after long-term ageing at 923 K for 1000 h (a); 3500 h (b); 5875 h (c); 10,987 h (d).

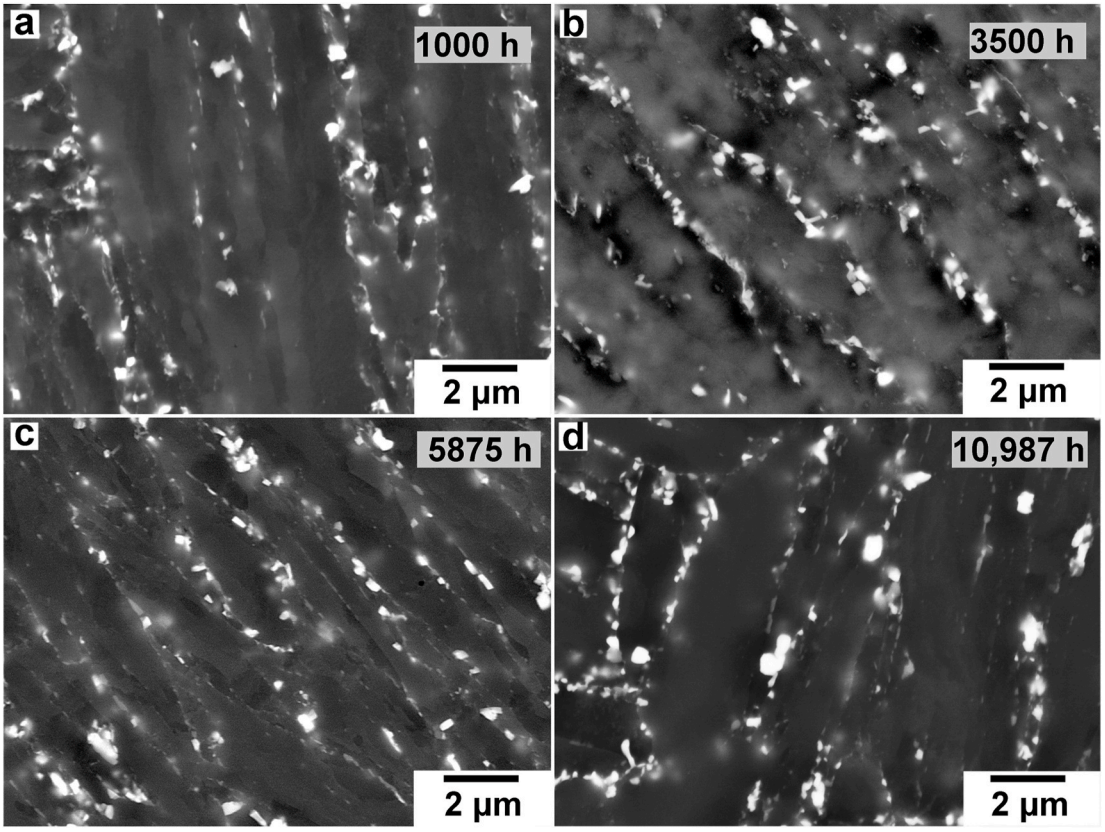

Fig. 3. SEM images of microstructure of the Re-containing steel studied after ageing at 923 K for 1000 h (a); 3500 h (b); 5875 h (c); 10,987 h (d).

The precipitation of W-rich particles and their significant growth were revealed after both creep and ageing at elevated temperature (Figs. 2–5, Tables 2 and 3). White particles in Figs. 3 and 5 corresponded to W-rich Laves phase particles were observed along both HABs of blocks, packets, PAGs and LABs of the martensitic laths. Under long-term ageing, the Laves phase particles rarely precipitated on the lath boundaries (Figs. 2 and 3). Major portion of Laves phase appeared on the HABs of blocks, packets and PAGs. The particles nucleated on the boundaries of PAGs and packets exhibited round shape, while the particles precipitated on the block boundaries had plate-like shape. Minor portion of Laves phase nucleated on the lath boundaries without a contact with a M_6C carbides and on semi-coherent longitudinal interfaces of M_6C carbides located on the lath boundaries [31,37,38]. These Laves phase particles exhibited rod-like shape and were susceptible to further dissolution due to large misfit and, therefore, high interfacial energy. This process was accompanied by extensive coarsening of the Laves phase particles located on the HABs of packets and PAGs (Fig. 3). Coarsening resulted in dissolution of the chains of the boundary particles along majority of the lath boundaries, while these chains retained on the block boundaries. After ageing for about 11,000 h, the coarse Laves phase particles with plate-like shape were in dominance (Figs. 2 and 3).

3.3. Evolution of TMLS and a dispersion of secondary phase particles during creep

Microstructures in the crept samples are shown in Figs. 4 and 5 and their parameters are summarized in Table 3. Up to second stage of tertiary creep, the average dimensions of the secondary phase particles after long-term ageing and creep are nearly the same (Tables 2 and 3). The main difference in a dispersion of secondary phase particles between creep and long-term ageing consisted in the sites for precipitation of the M_6C/Laves phase particles [31]. Creep highly promoted the nucleation of M_6C carbides on the $M_{23}C_6$/α-Fe interfaces followed by nucleation of the fine Laves phase particles with equiaxed shape on the M_6C/α-Fe interfaces of the hybrid $M_6C/M_{23}C_6$ particles [31]. As a result, the major portion of Laves phase nucleated on the M_6C/α-Fe interfaces of the hybrid particles [31] under transient creep. A portion of Laves phase nucleated on the lath boundaries with and without a contact with carbides [31] was 0.5 and 0.4 after creep and ageing, respectively (Figs. 2 and 4). Therefore, the strain-induced formation of the hybrid $M_6C/M_{23}C_6$ particles promoted the nucleation of Laves phase on the lath boundaries [31]. The density of Laves phase located on the lath boundaries in the present steel was significantly higher than that for the 9% Cr-3% Co-2% W steel with low C content [39]. Moreover, an increase in the boron content and a decrease in the nitrogen content promoted the nucleation of the Laves phase particles on the LABs [12]. $M_{23}C_6$ carbides additionally precipitated on the lath boundaries during creep up to thermodynamically equilibrium volume fraction as in other high-Cr steels with the increased boron content [12]. As a result, the dense chains of $M_{23}C_6$ carbides and Laves phase appeared along the lath boundaries and retained up to rupture.

The TMLS partially transformed into the subgrain structure, wherein the average size of martensitic laths/subgrains dramatically increased up to 1 μm (Fig. 4d, Table 3). The average size of the martensitic laths in the gauge portion insignificantly increased up to 600 nm during 440 h of creep, wherein the TMLS retained (Fig. 4a–c, Table 3). The precipitation of $M_{23}C_6$ carbides and Laves phase on the lath/subgrain boundaries stabilized this structure up to the onset of the second stage of tertiary creep (Figs. 4 and 5, Table 3). Well-defined strain-induced coarsening of $M_{23}C_6$ carbides was found at the second stage of tertiary creep and was accompanied by a significant decrease in the dislocation density and coarsening of the subgrains and laths (Fig. 4c and d, 5c,d, Table 3). Strain-induced coarsening of M(C,N) carbonitrides and Laves phase was

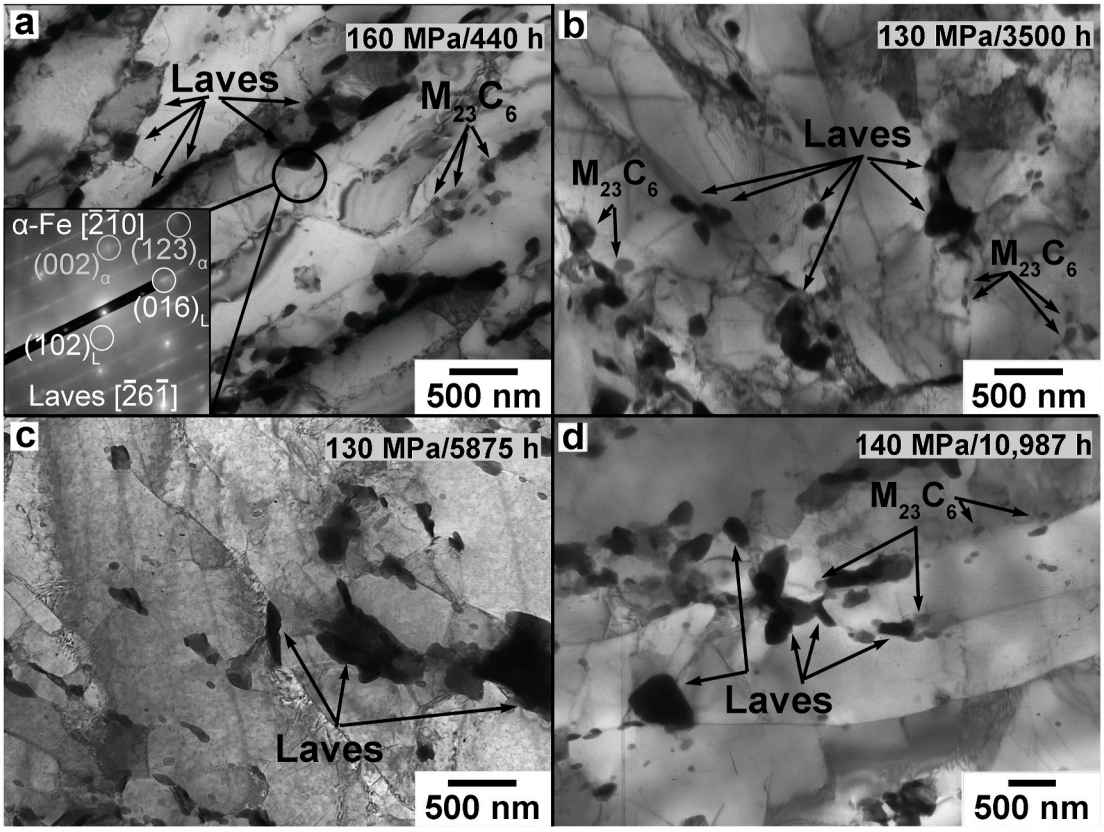

Fig. 4. TEM images of microstructure of the steel studied after creep tests at 923 K under the stress of 160 MPa, 440 h (a); 130 MPa, 3500 h (b); 130 MPa, 5875 h (c); 140 MPa, 10,987 h (d).

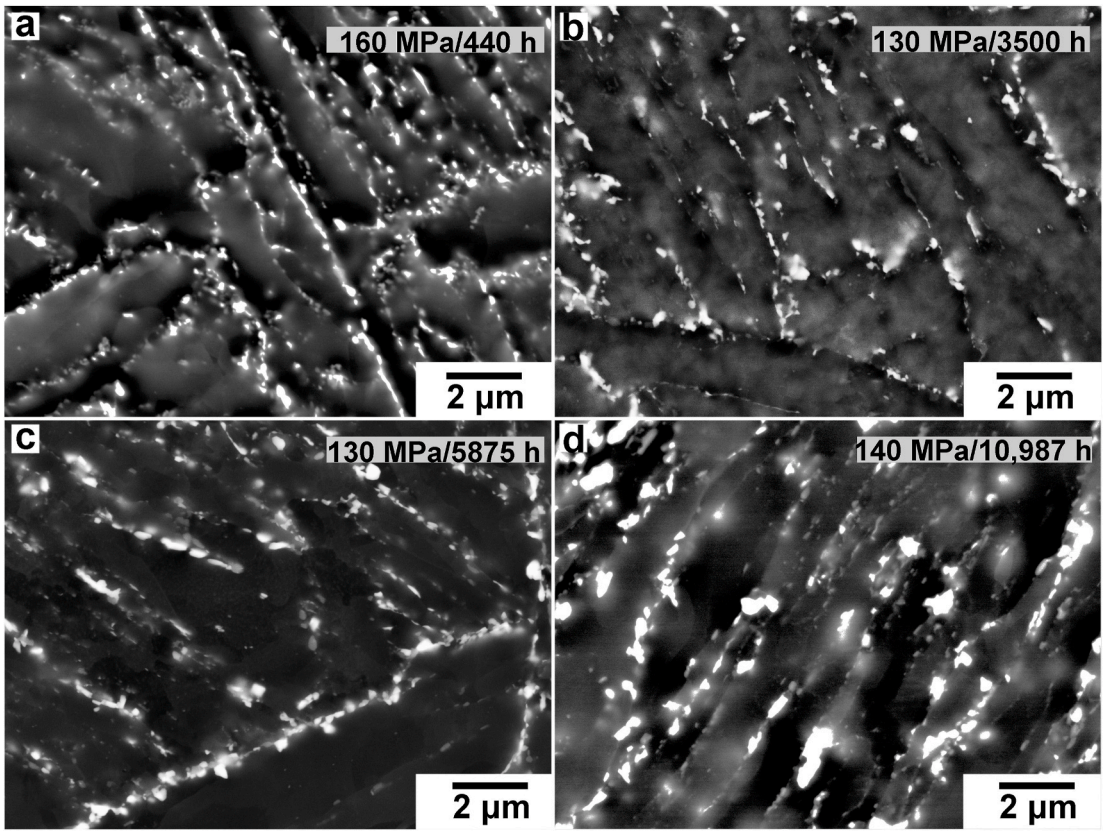

Fig. 5. SEM images of microstructure of the steel studied after creep tests at 923 K under the stress of 160 MPa, 440 h (a); 130 MPa, 3500 h (b); 130 MPa, 5875 h (c); 140 MPa, 10,987 h (d).

Table 3
Structural parameters of the 10% Cr-3% Co-3% W-0.2% Re steel after some crept states at different conditions at 923 K in the gauge sections.

Creep condition	Lath size, nm	Subgrain size, nm	ρ_{disl}, × 10^{14} m^{-2}	The mean size of particles, nm		
				$M_{23}C_6$	Nb (C, N)	Laves phase
160 MPa/ 440 h	573 ± 20	600 ± 20	1.03 ± 0,1	81 ± 10	50 ± 5	106 ± 20
130 MPa/ 3500 h	600 ± 20	650 ± 20	0.94 ± 0,1	89 ± 10	50 ± 5	150 ± 20
130 MPa/ 5875 h	650 ± 20	650 ± 20	0.93 ± 0,1	88 ± 10	50 ± 5	136 ± 20
140 MPa/ 10,987 h	1220 ± 20	1100 ± 20	0.17 ± 0.01	120 ± 10	50 ± 5	200 ± 20

insignificant (Tables 2 and 3).

3.4. Depletion of solute W and precipitation of Laves phase during creep and ageing

The W depletion from the solid solution occurred with increasing time and was accompanied with the precipitation of Laves phase (Fig. 6a) during creep and long-term ageing at 923 K. Kinetics of W depletion under creep and ageing conditions were nearly similar. Strain shifted the Laves phase precipitation to lower time (Fig. 6). The onset of W depletion was observed after 10 and 20 h under creep and long-term-ageing, respectively. The depletion of W from ferrite and the precipitation of Laves phase occurred with a high rate in the time interval ranging of 100–500 h. According to simulation using TC-Prisma (Fig. 6a), this phase transformation terminated at 500 and 1000 h under creep and long-term ageing, respectively. Therefore, strain accelerates the precipitation of Laves phase.

The W depletion from the solid solution $f(W)$ can be described as [27]:

$$f(W) = 2.17\exp(-0.0033t) \text{ during creep} \quad (3)$$

$$\text{and } f(W) = 2.38\exp(-0.0083t) \text{ during ageing} \quad (4)$$

where t is ageing/creep time in h.

On the base of comparison of the theoretically predicted curves with experimental data (particle sizes measured using TEM in the gauge and grip sections of the crept specimens), the values of the interfacial energy of the Laves phase particles were estimated (Fig. 6). The effects of time on volume fractions and average sizes of the Laves phase particles were well described by simulation (Fig. 6a and b) using an interfacial energy of 0.72 and 0.78 J m^{-2} for creep and long-term ageing, respectively. The Laves phase particles nucleated on the hybrid particles located on the lath boundaries during creep were characterized by lower interfacial energy. These particles were more resistant to coarsening than those nucleated on the lath boundaries or on the semi-coherent longitudinal interface of M_6C carbides located on the lath boundaries during long-term ageing [31]. Strain-induced acceleration of W depletion was attributed to easy formation of the hybrid $M_6C/M_{23}C_6$ particles that promoted nucleation of the Laves phase particles on their interfaces [31]. The equilibrium volume fraction of Laves phase was the same for creep and long-term ageing. According to the prediction of TC-Prisma software, the equilibrium W content in the ferritic matrix of 1.24 wt% and the volume fraction of Laves phase of 1.6% were reached after 500 h of creep and 1000 h of ageing. So, creep accelerates kinetics of the precipitation of Laves phase but has no effect on its volume fraction. M. Hattestrand et al. [40] supports this conclusion reported no difference in the volume fraction of Laves phase between aged and crept samples of a

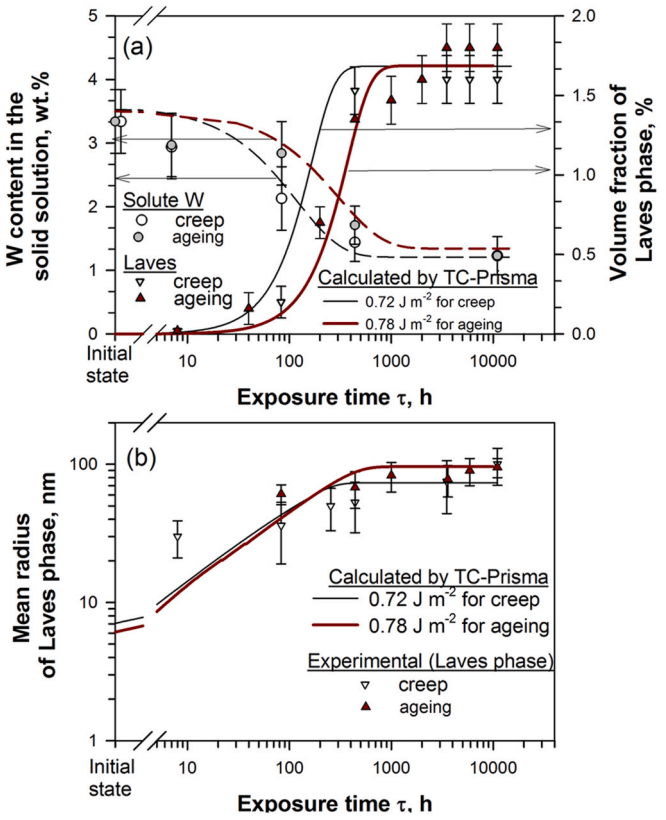

Fig. 6. Correlation between depletion of W from the solid solution and increase in volume fraction of Laves phase (a); time dependence of the Laves phase particle size (b) during creep and ageing. Circle grey and white points correspond to solute W in the ferrite matrix after creep (in the gauge sections) and ageing (in the grip portions), respectively; white triangle down and dark red triangle up are the experimental Laves phase volume fraction (a) and mean size (b) after creep and ageing, respectively; black and dark red long dash lines are calculated curves obtained by Prisma-software for the model steel and correspond to creep and ageing conditions, respectively. (For interpretation of the references to colour in this figure legend, the reader is referred to the Web version of this article.)

P92 steel at 873 K.

3.5. Size distribution and chemical composition of Laves phase

The difference in coarsening behaviour of Laves phase precipitated during long-term ageing and creep is illustrated by dimension distribution of these particles (Figs. 7 and 8). Under long-term ageing, the Laves phase particles precipitated on the lath boundaries with a lower rate at ≤ 440 h. Further ageing led to progressive dissolution of these fine particles; portion of the Laves phase particles with dimensions ≤50 nm gradually decreased with increasing duration of long-term-ageing. Concurrently, the fast growth of the Laves phase particles located on the HABs took place; the coarse particles with dimensions ≥500 nm appeared.

Creep strain promoted the formation of the Laves phase particles with dimensions ranging from 25 to 75 nm due to their nucleation on the hybrid carbide particles [31]. These particles were resistant to coarsening and retained up to rupture. Their growth and/or dissolution occurred with a low rate. The Laves phase particles located on the boundaries of packets and PAGs showed coarsening with a high rate accompanied by partial dissolution of Laves phase nucleated on the hybrid carbide particles [31]. This process led to the appearance of the coarse Laves phase particles with dimensions ranging from 250 to 500 nm. Superposition of slow coarsening of the fine particles located on the lath boundaries and fast growth of the particles located on HABs was described by Gaussian distribution, which fits the experimental data well, under all creep and ageing conditions.

The red lines in Figs. 7 and 8 described the size distribution obey equation of normal Gaussian distribution:

$$f = \frac{1}{\sqrt{2\pi\sigma^2}} \times \left(-\frac{1}{2} \times\right) \frac{|x - x_0|^2}{\sigma^2} \quad (5)$$

where 12πσ2 is normalization constant, x_0 is mean value, σ2 is variance. The peak width expanded from 47 for 440 h to 94 for 10,987 h in the crept samples and from 80 for 1000 h to 89 for 10,987 h in the aged samples. The onset of Laves phase coarsening during ageing was characterized by expanded size distribution, whereas the width of size distributions after 10,987 h for creep and long-term ageing were considered to be similar discarding the large Laves phase particles in Fig. 7d. The Gaussian peak corresponded to the mean x_0 (Figs. 7 and 8). The values of x_0 from Eq. (5) were similar to the average sizes of Laves phase dav calculated by TEM and SEM of foils and TEM of carbon replicas (Figs. 2–5). The ratio of x0 dav decreased from 1.12 for 440 h and 3500 h to 1.08 for 5875 and 10,987 h of creep, i.e. x0 = 3.5πdav for 440 h and 3500 h and x0 = 3.4πdav for 5875 and 10,987 h of creep that was close to the mean equivalent diameter (d_{corr}) estimated by L. Korcakova et al. [41], which was described as dcorr = 4πdobs. The similar ratio was observed for long-term ageing.

The chemical compositions of Laves phase after creep and long-term ageing were essentially the same (Fig. 9). The ratio of W: Σ(Fe,Cr) in Laves phase was 1.5 : 1 after all creep tests. After 3500 h of creep test at 650 °C/130 MPa (interrupted test), Cr content in the Laves phase particles insignificantly increased at the expense of Fe, wherein ratio W/Σ(Fe + Cr) remained as 1.5 : 1. A further increase in creep time led to decreasing Cr content and increasing Fe content in Laves phase. Moreover, the chemical composition of Laves phase after 10,987 h of creep or ageing absolutely corresponded to the composition predicted by Thermo-Calc software (Fig. 9).

4. Discussion

4.1. Precipitation kinetics of Laves phase

Experimental data presented in this work and the companion article [31] show that the precipitation sequence

$$\alpha\text{-Fe} \rightarrow M_{23}C_6 \rightarrow M_6C \rightarrow \text{Laves phase} \quad (6)$$

Occurs in the Re-containing 10% Cr-3% Co-3% W steel. The precipitation of $M_{23}C_6$ carbide precedes the precipitation of W-rich M_6C carbide [31]. Schematic illustration is shown in Fig. 10. The α-Fe → M_6C transformation occurs through nucleation of M_6C carbide on (1) the $M_{23}C_6$/α-Fe interfaces and (2) the lath boundaries during creep and long-term ageing (Fig. 10a and b). The M_6C → Laves phase transformation occurs through nucleation on (1) M_6C/α interfaces and (2) the lath boundaries followed by growth of Laves phase by the expense of ferrite or M_6C carbides, respectively (Fig. 10a and b). In this work, no growth of Laves phase at the expense of $M_{23}C_6$ carbide [42] was found. The $M_{23}C_6$/α-Fe interfaces play a role of the nucleation sites for W-rich M_6C/Laves phase [31]. The additional precipitation of $M_{23}C_6$ carbides up to thermodynamically equilibrium volume fraction takes place under creep that increases the number of nucleation sites for the W-rich phases on the lath boundaries, since most part of $M_{23}C_6$ carbides precipitates on them [12,25,31]. In general, $M_{23}C_6$ is not a transition phase in precipitation sequence (6). However, this carbide plays a crucial role in the precipitation of Laves phase and its contribution to creep resistance [12]. In addition, the α-Fe → Laves phase transformation occurs independently through heterogeneous nucleation of Laves phase on LABs and HABs. Thus, the Laves phase particles precipitate on the boundaries of laths, blocks, packet and PAGs with or without contact with these

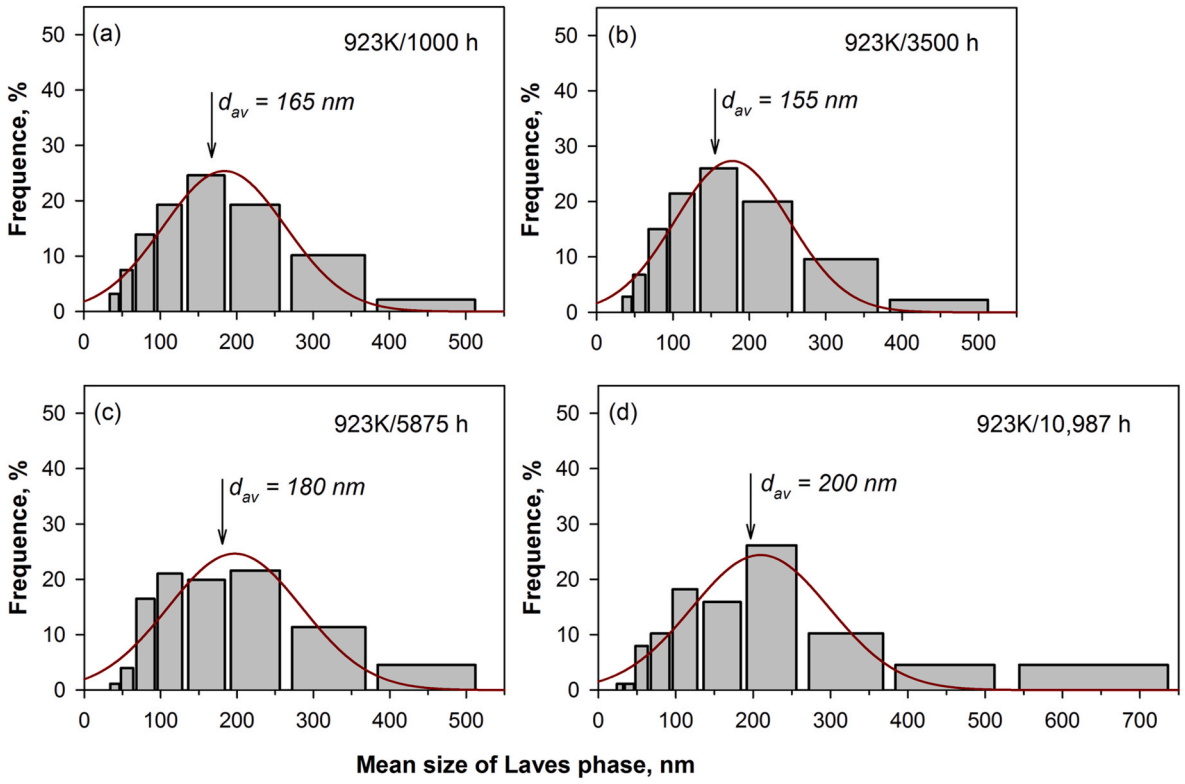

Fig. 7. Size distributions of the Laves phase particles after ageing at 923 K for 1000 h (a), 3500 h (b), 5875 h (c) and 10,987 h (d). The red lines represent normal Gaussian distribution. (For interpretation of the references to colour in this figure legend, the reader is referred to the Web version of this article.)

carbides; strain promotes nucleation of this phase on the lath boundaries (Fig. 10b) [5–7,9–12,31] and (6) represents the sequence of precipitation of nucleation sites ($M_{23}C_6$), transition (M_6C) and thermodynamically stable (Laves) phases.

Growth of the Laves phase particles is anisotropic (Fig. 10c). A Laves phase particle precipitated at a boundary exhibits a rational orientation relationship (OR) with one grain/lath matrix, its interfaces with this matrix are semi-coherent, and the particle grows toward the adjacent grain/lath with which it does not have this OR; its incoherent interface has a high mobility [31,39,43]. However, the growth of the Laves phase particle may occurs by consuming M_6C carbides due to migration of semi-coherent interface (Fig. 10b and c) [10,16,31,44]. The growth of the Laves phase particles may be isotropic if a particle grows concurrently into both the adjacent grain/lath matrix and M_6C carbide (Fig. 10b and c). Since thermodynamically equilibrium volume fraction of Laves phase calculated by Prisma is ~1.6%, no mutual impingement of growing particles of Laves phase occurs. Therefore, precipitation kinetics of Laves phase involves nucleation and growth. However, boundary $M_{23}C_6$ carbides may block the growth of the Laves phase particles along a boundary. Impingement of the Laves phase particles and $M_{23}C_6$ carbides may occur due to their concurrent precipitation and growth. The overlap of these two different types of particles leads to hard impingement [45–47]. No soft impingement due to the overlap of diffusion fields surrounding the growing particles [45–48] can appear since the chemical compositions of Laves phase and $M_{23}C_6$ carbide are different.

Temporal dependencies of the number density of Laves phase are presented in Fig. 11. Creep strongly promotes the nucleation of Laves phase due to the additional precipitation of $M_{23}C_6$ carbides on the lath boundaries. The number density of Laves phase after creep (2.45×10^{19} m^{-3}) is higher by a factor of ~3 than that after long-term ageing (Fig. 11). Ageing for 1000 h is characterized by extensive coarsening of Laves phase; no increase in the number density of Laves phase is observed (Fig. 11). Under creep and long-term-ageing at $t \geq 500$ h and $t \geq 1000$ h, respectively, the "pure" growth of Laves phase particles, which is not accompanied by the concurrent additional nucleation, takes place before steady-state creep stage (Fig. 1b).

The critical nucleus diameter for nucleation of Laves phase, d_{cr}, can be evaluated by Refs. [36,44–48]:

$$d_{cr} = \frac{4\gamma V_m}{\Delta G_m} \tag{7}$$

where ΔG_m is the molar free energy change due to precipitation of Laves phase (2329.38 J mol^{-1} at 923 K calculated by the Thermo-Calc software), γ is the energy of Laves phase/α-ferrite interface (0.72 J m^{-2} for creep and 0.78 J m^{-2} for ageing (Fig. 6)), V_m is the molar volume of the Laves phase (7.9×10^{-6} m^3 mol^{-1} at 923 K obtained by the Thermo-Calc software). The high values of d_{cr} of 9.8 and 10.6 nm were obtained for creep and long-term ageing, respectively. These values are in agreement with those obtained by Isik et al. [37,38] and are higher than those reported by Prat et al. [49,50]. It is obviously that this diameter is too high for homogeneous nucleation [45,46]. Q. Li [43] showed that nucleation of Laves phase with coherent interfaces on the lath boundaries may occur due to a relatively low misfit of 2.7%. The formation of Laves phase with OR reported in Ref. [43] was not detected in the present steel [31]. However, we may assume that Laves phase appears as a nucleus with coherent boundaries. Low energy of coherent interface is evaluated as 0.1 J m^{-2} [49,50]; appropriate value of critical nucleus dimension is ~1.4 nm in accordance with Eq. (7). This value is reasonable for coherent interfaces with ORs characterized by relatively large misfits of ~7% with ferritic matrix [31]. However, growth of this nucleus inevitably leads to loss of coherency.

4.2. Activation energy of Laves phase precipitation

The Johnson–Mehl–Avrami–Kolmogorov (JMAK) phenomenological model can predict the kinetics of isothermal phase transformation proceeded through random or uniform nucleation and isotropic growth

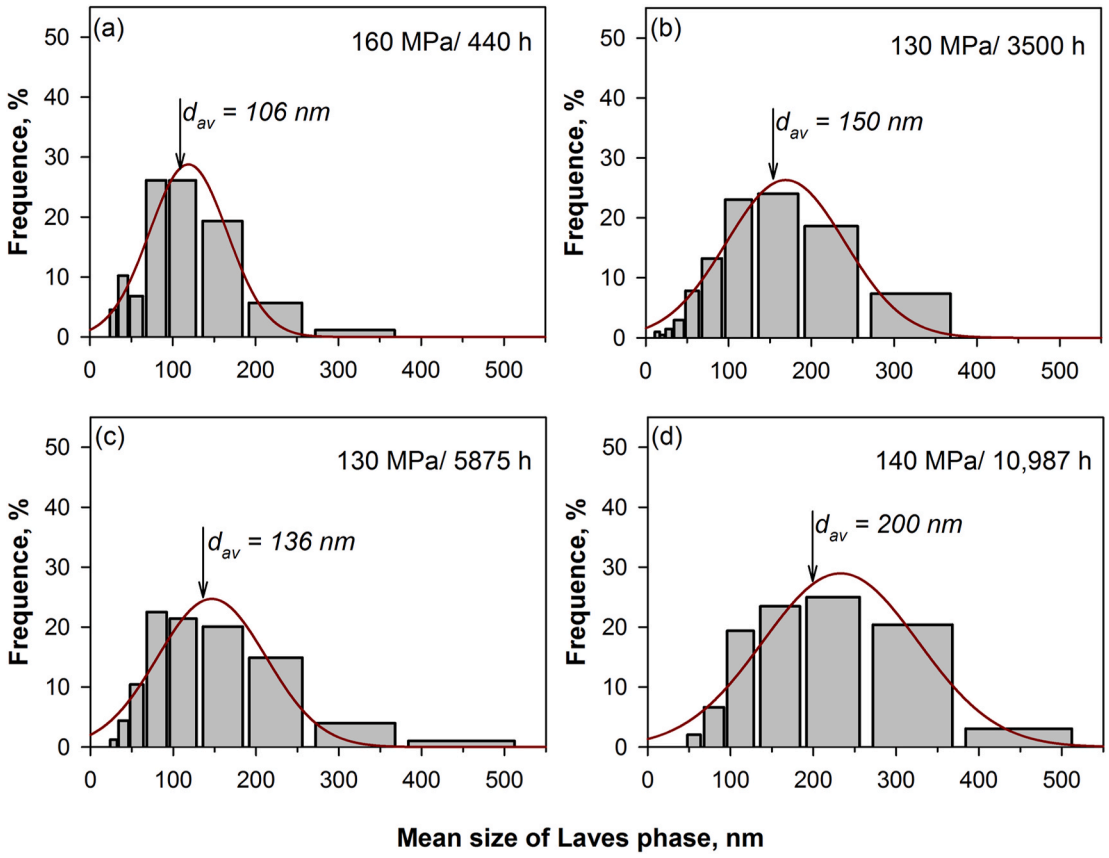

Fig. 8. Size distributions of the Laves phase particles after creep tests at 923 K under 160 MPa, 440 h to rupture (a); 130 MPa, 3500 h (b); 130 MPa, 5875 h (c); 140 MPa, 10,987 h to rupture (d). The red lines represent normal Gaussian distribution. (For interpretation of the references to colour in this figure legend, the reader is referred to the Web version of this article.)

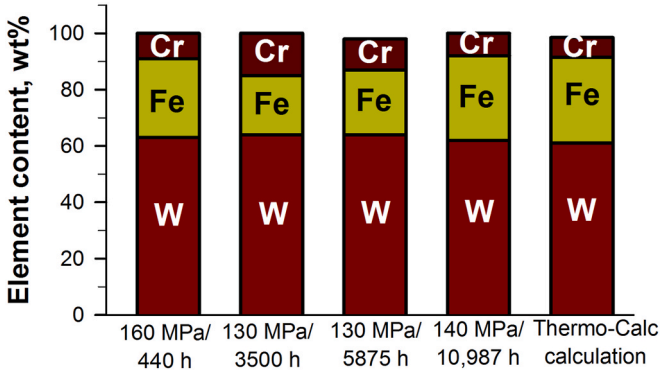

Fig. 9. The change in the chemical composition of Laves phase after creep tests with different applied stresses and durations.

followed by impingement of growing particles that shields the process [43–48]. Kinetic of the Laves phase precipitation is described by JMAK model despite heterogeneous nucleation followed by anisotropic growth and no mutual impingement due to the overlap of growing particles [51–54]. The portion of precipitated Laves phase can be described by JMAK model as [43–48,51–55]:

$$Y = 1 - \exp(-(t/t_0)^n) \tag{8}$$

where n is the Avrami exponent, which is depended on the nucleation mechanism and growth type, t_0 is a time constant, Y is determined as a ratio $Y=V/V_{eq}$ between volume fraction, V, at time of t and equilibrium volume fraction, V_{eq} = 1.6% calculated by TC- Prisma at 923 K.

Inspection of Fig. 12 shows that the precipitation behaviour of Laves phase obeys JMAK equation. The Avrami exponent n ranging from 1.5 to 2.5 describes mixed or Avrami nucleation and particle growth controlled by lattice diffusion [45–47]. The Avrami exponent n ranging from 0.5 to 1.5 is indicative for a decreasing nucleation rate with increasing time, t; the heterogeneous nucleation on the boundaries and the particle growth are controlled by grain boundary diffusion [53,55]. The following results are obtained at 923 K: $t_0 = 497$ h or 1.8×10^6 s and 1001 h or 3.6×10^6 s for creep and ageing, respectively, and $n = 1.07$ and 1.21 for creep and ageing, respectively (Fig. 12).

Following the nucleation theory suggested by J.W. Christian [44–46,51], the time constant (t_0) is given by

$$\left(\frac{1}{t_0}\right)^n = 2D\left(\frac{4}{3}\pi N\right)^{\frac{2}{3}}\left(\frac{C^m - C^\alpha}{C^\beta - C^\alpha}\right)^{\frac{1}{3}} \tag{9}$$

where N is a nucleation rate per unit volume calculated using Prisma and Thermo-Calc software ($2.61 \cdot 10^{26}$ m^{-3} at a lath width of 500 nm); Cm = 719 mol m^{-3} is initial solute W concentration in matrix, Cα = 7.5×10^2 mol m^{-3} and Cβ = are 40563.5 mol m^{-3} are equilibrium concentrations of W in α-ferrite and Laves phase, respectively, at 923 K calculated by Thermo-Calc software. D is interdiffusion coefficient of W solute can be written in the form:

$$D = D_O \exp\left(-\frac{Q}{RT}\right) \tag{10}$$

where Q is activation energy for the particle growth; R is gas constant, T is temperature in K and D_0 is the frequency factor. The $D_0 = 1.51 \times 10^{-2}$ m^2 is the same for lattice diffusion and the grain boundary diffusion.

The Q values for nucleation are calculated as 116 and 138 kJ mol^{-1}

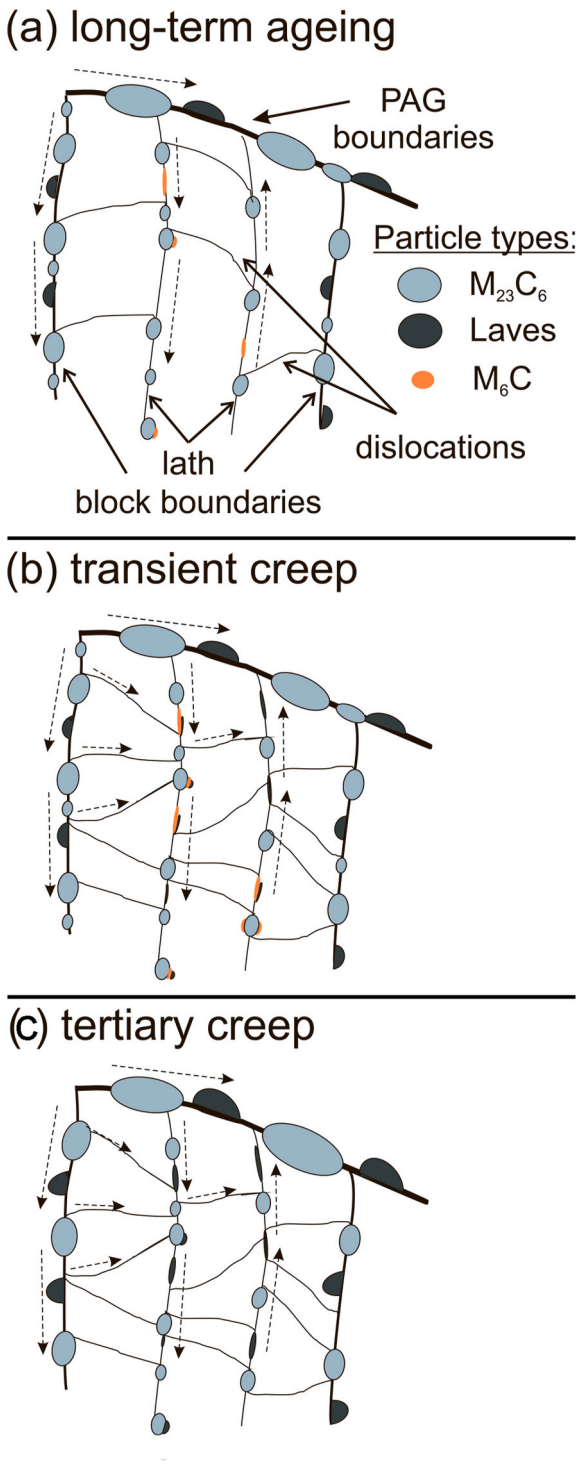

Fig. 10. Schematic illustration of the microstructural evolution of a dispersion of secondary phase particles and TMLS during long-term ageing (a), transient creep (b) and tertiary creep (c). Arrows indicate the diffusion flows of atoms to the boundary particles.

for creep and long-term ageing, respectively, taken $D = 1.59 \times 10^{-23}$ m^3 s^{-1} as the grain boundary diffusion coefficient, for 923 K [56]. The D values of W in ferromagnetic α-Fe (A_{c2} is ~1053 K for this type of steels [57]) reported in works [58–60] are distinctly different. The values of activation energy are less than half of the activation energy for volume diffusion of W ($Q^F = 245$ kJ mol^{-1}) in ferromagnetic state [58–60]. We may assume that nucleation process is controlled by grain boundary or pipe diffusion of W solute since their activation energies are usually the

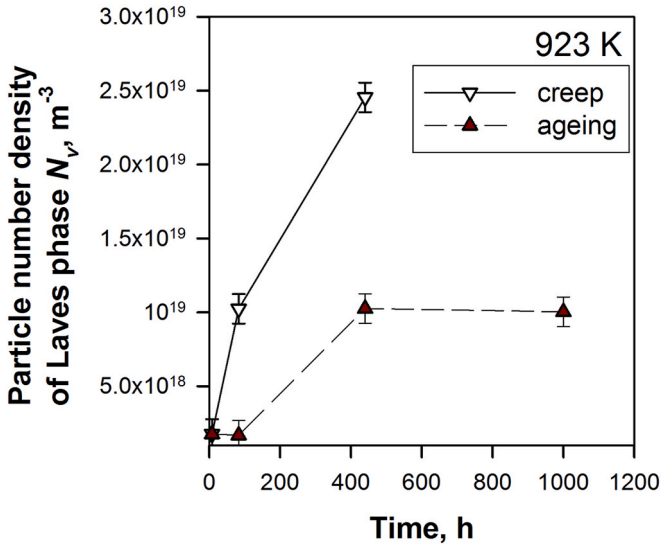

Fig. 11. Effect of creep/long-term ageing time on the number density of Laves phase.

same despite the fact that Cermak et al. [57] reported a value of 195 kJ mol^{-1} as activation energy for grain boundary diffusion of W solutes in α-ferrite. For the Co-modified P911-type steel, the activation energy for growth of the Laves phase particles is 60 kJ mol^{-1} [32], which is also less than the activation energy for volume diffusion of tungsten [58–60]. K. Miyata [52] suggested the temperature of 923 K promoting the precipitation of W-rich particles (M_6C carbides or Laves phase) is not enough to induce the self-diffusion of W. Moreover, creep deformation facilitates the grain boundary diffusion or pipe diffusion due to decreasing the activation energy. This seems that decreasing the activation energy for W diffusion and for the particle growth during creep is caused by activation of the grain boundary dislocation sources generating new dislocations. New dislocations are the additional short-circuits ways for tungsten diffusion along grain/subgrain boundaries that leads to higher amount of nucleation sites for W-rich Laves phase during creep (Fig. 10).

4.3. Coarsening of Laves phase during creep and long-term ageing

A kinetic law for growth of Laves phase due to diffusion-controlled coarsening is given by Lifshitz-Slyozov-Wagner (LSW) relationship [39,51,53,54,60–63]:

$$d^m - d_0^m = K_p(t), \tag{11}$$

where d is an average particle dimension at a time of t, d_0 is the average particle size at the onset of the coarsening process (10 nm for both creep and ageing conditions from Eq. (7)), K_p is coarsening rate constant, the growth exponent m depends on the coarsening mechanism and is $m = 3$ for lattice diffusion, $m = 4$ for grain boundary diffusion and $m = 5$ for pipe diffusion coarsening. The $m = 4$ provides the best fit of experimental data to linear dependences (Fig. 13), and, therefore, Ostwald ripening of Laves phase is controlled by grain boundary diffusion [39]. Lattice and pipe diffusions are not important for coarsening of Laves phase in this steel.

The coarsening rate constant, K_p, is determined by the following equation [62–65]:

$$K_p = \frac{8}{9} D_{GB} \frac{\gamma C^{\alpha} s \delta V_m^2}{GRT} \frac{< v(\varphi) >^4}{\nu(\varphi)} \tag{12}$$

where ceces, δ are the segregation factor and the grain boundary width, respectively, G is geometrical factor (0.657), υϕ and νϕ are parameters, which were taken from the plots reported by A. Ardell [64], ϕ is volume fraction, R is gas constant, and T is temperature.

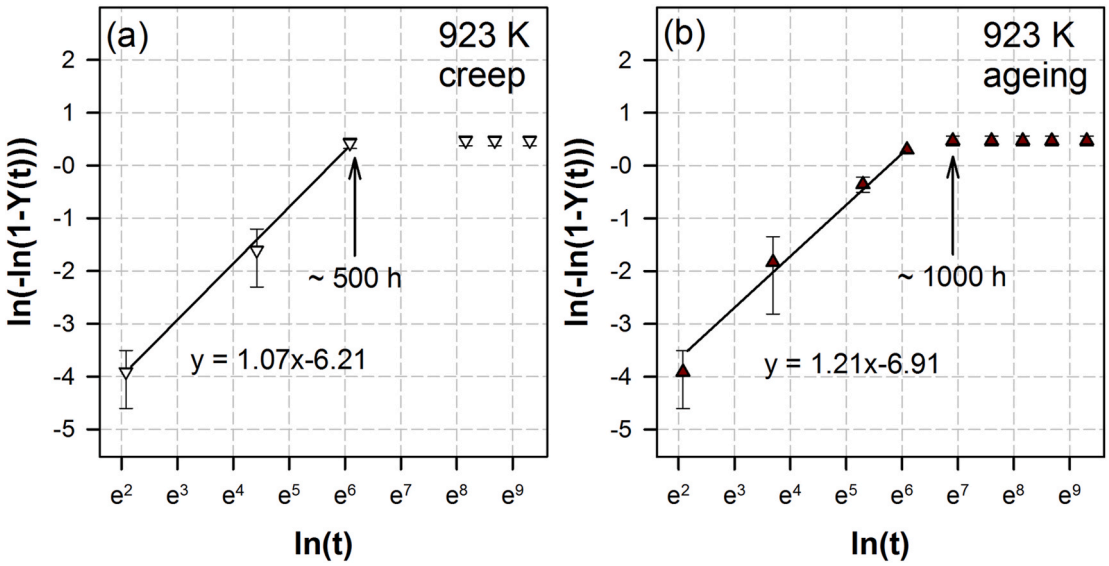

Fig. 12. Evaluation of time exponent n based on the quantification results of the Laves phase particle fraction after creep tests (a) and ageing (b) at 923 K.

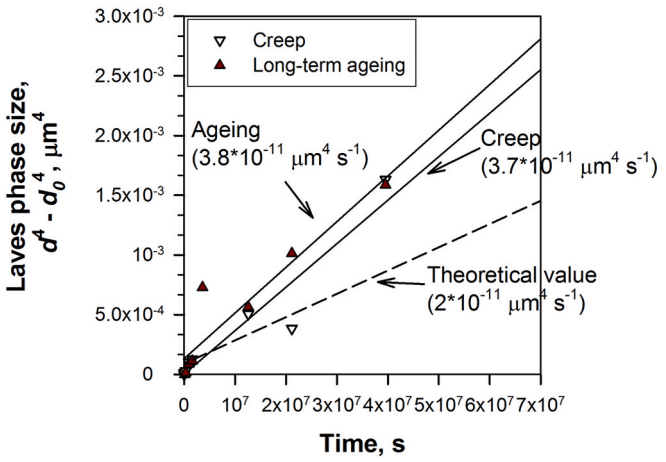

Fig. 13. The time dependence of the Laves phase particle size during creep and ageing. Numbers indicate the coarsening rate constant.

The theoretical value of the coarsening rate constant of Laves phase for the Re-containing 10% Cr-3% Co-3 W steel of $2{\cdot}10^{-11}$ μm^4 s^{-1} for both creep and ageing (Fig. 13) is lower than experimental values of $3.7{\cdot}10^{-11}$ and $3.8{\cdot}10^{-11}$ μm^4 s^{-1} for creep and ageing, respectively. The difference between experimental and theoretical values is attributed to the fact that growth of the Laves phase particles located on the lath boundaries and on the HABs of blocks, packets and PAGs occurs in nearly independent manner. The Laves phase particles located on the HABs ($d \geq 100$ nm in Figs. 7 and 8) are susceptible to coarsening that leads to appearance of the particles with dimensions >200 nm. The Laves phase particles located on the lath boundaries dissolve with a low rate. This process gives insignificant contribution to growth under creep, since pipe diffusion could not provide a sufficient diffusion flux from these fine particles located on the LABs to the large particles located on the HABs (Fig. 10).

Similar growth behaviour of Laves phase during both creep and ageing is expected because the main criteria for the onset of particle coarsening (the volume fraction, the solute of W in the solid solution, tungsten grain boundary diffusivities and etc.) are the same for both creep and ageing conditions. However, the size distribution of Laves phase particles at the beginning of coarsening during ageing is wider (Figs. 7 and 8). This fact indicates that the conditions such as the volume fraction, amount of nucleation sites, the solute of W in the solid solution, tungsten grain boundary diffusivities have a greater influence on the coarsening rate constant than the width of size distribution of Laves phase particles [66]. A bit higher value of the coarsening constant rate during ageing is accompanied with a higher value of interfacial energy between Laves phase and ferrite and lower value of the nucleation sites for Laves phase. The similar results were reported by I. Fedorova et al. [39] for the 9% Cr-3% Co-2% W steel with low C content. However, the effect of creep deformation on the growth of Laves phase in the Re-containing steel is weaker than that in the 9% Cr-3% Co-2% W steel with the low C content [39].

As shown by the comparison of a P92-type steel and C-depleted 9% Cr steel [39,54,55], the grain boundary diffusion plays an important role in the Ostwald ripening of the Laves phase precipitates. However, kinetic of Laves phase growth in the Re-containing 10% Cr-3% Co-3% W steel with the low N content has distinct features. Re in matrix effectively slows down diffusivity that suppresses the nucleation and growth of Laves phase assisted by lattice diffusion of W solutes. In the same time, tungsten content of ~3 wt% provides increased driving force for precipitation of M_6C carbides and Laves phase. Creep promotes additional precipitation of $M_{23}C_6$ carbides on the lath boundaries evolving numerous sites for heterogeneous nucleation of M_6C carbides and Laves phase [31]. As a result, under creep, a half of these particles precipitate on the lath boundaries and their nucleation occurs with a high rate [31]. The further growth of Laves phase located on the lath boundaries and on the HABs of PAGs, packets and blocks occurs nearly independent since distance for W flux between these two types of particles is high (~500 nm) (Fig. 10) and lattice diffusivity of W at 923 K is low. As a result, dense chains of Laves phase on the lath boundaries retain up to high creep rupture time giving a significant contribution to creep behaviour.

4.4. Laves phase and creep behaviour

It is known [5,6,8,68–70] that the martensite laths are single crystals lying parallel to the $\{110\}_{\alpha'}$ planes. In fact, the laths are 1D sub-units of a block with the longest axis located along the closed-packed direction of the martensite [5,67,68]. Two types of dislocation glide may be operative within the lath (Fig. 10). If slip plane is parallel to the habit plane and, therefore, two possible $<111>_{\alpha'}$ slip directions intrinsically proceed parallel to the lath interfaces, this slip system is termed as the in-lath system [69,70]. The precipitation of the Laves phase particles on the lath boundaries during transient creep increases the number of

obstacles for the in-lath dislocation glide [6,8] in addition to boundary $M_{23}C_6$ carbides (Fig. 10b). The in-lath dislocation slip imperatively leads to attractive interaction between a gliding dislocations and the Laves phase particles precipitated on the lath boundaries giving the main contribution to threshold stress [6,7,71,72]. The precipitation of the Laves phase chains on the lath boundaries during transient creep (Fig. 10b) restricts the ability of gliding dislocations to rearrangement by climb that hinders the knitting reaction between the lattice dislocations and the lath boundaries. In addition, lattice dislocations gliding through in-lath way interact with the boundary particles and could not bypass matrix obstacles by general climb [7]. These dislocations have to overcome M(C,N) carbonitrides by detachment process [6]. The boundary $M_{23}C_6$ carbides and Laves phase as well as matrix M(C,N) carbonitrides with incoherent interfaces are bypassed by dislocations via a sequential process consisting of local climb, glide of climbing portion of lattice dislocation along the interface boundary and subsequent detachment [6,7,72]. These processes may exert threshold stress [7,72]. Thus, the precipitation of the Laves phase particles on the lath boundaries is responsible for a decrease in the creep rate down to 10^{-10} s^{-1} at 130 and 140 MPa during transient creep stage (Figs. 1 and 10b) [7,12,26,27].

Both the precipitation of the major portion of Laves phase on the lath boundaries and the formation of the Laves phase particles located on the HABs of PAGs and packets with dimensions $\leq$500 nm (Fig. 8d) due to Ostwald ripening prevent the premature fracture due to extensive cavitation in the vicinity of the coarse Laves phase particles. As a result, the steel exhibits sufficient ductility (Fig. 1). Thus, Re additives slowing down diffusion of tungsten in ferrite promote the precipitation of Laves phase on the lath boundaries and hinder dissolution of these particles [26]. The Re-containing high-Cr steel with the high boron and low nitrogen contents is a unique material, in which the precipitation of Laves phase on the lath boundaries during transient creep stage provides superior creep resistance.

5. Conclusions

The precipitation and coarsening of Laves phase in the Re-containing 10% Cr-3% Co-3% W creep resistant steel was examined during creep and long-term ageing at 923 K under the applied stresses of 200–130 MPa for the highest rupture time of ~11,000 h. The main summary can be written as follows:

1. Creep accelerates depletion of W from ferrite and promotes the precipitation of Laves phase on the lath boundaries. Dense chains of Laves phase and $M_{23}C_6$ carbides evolve on the lath boundaries during transient creep stage that decreases the creep rate down to 10^{-10} s^{-1} at 130 and 140 MPa.
2. Both nucleation and growth of Laves phase are controlled by grain boundary diffusion of tungsten solutes. For creep and ageing at 923 K, the activation energies for the Laves phase particle growth are 116 and 138 kJ mol^{-1}, respectively, which are approximately twice lower than the activation energy for volume diffusion of tungsten (215 kJ mole-1). Creep deformation facilitates the grain boundary diffusion or pipe diffusion due to decreasing the activation energy.
3. Ostwald ripening of Laves phase located on the HABs and on the lath boundaries occurs nearly independent; the chains of nanoscale Laves phase retain on the lath boundaries even at a rupture time of about 11,000 h. No strain-induced coarsening of Laves phase is revealed.

Data availability

The raw/processed data required to reproduce these findings cannot be shared at this time as the data also forms part of an ongoing study.

CRediT authorship contribution statement

A. Fedoseeva: Conceptualization, Methodology, Software, Investigation, Visualization, Writing – original draft, Writing – review & editing, Funding acquisition. **I. Nikitin:** Investigation, Formal analysis, Visualization. **N. Dudova:** Investigation, Formal analysis. **R. Kaibyshev:** Supervision, Methodology, Writing – original draft.

Declaration of competing interest

The authors declare that they have no known competing financial interests or personal relationships that could have appeared to influence the work reported in this paper.

Acknowledgments

This study was financially supported by the Russian Science Foundation, under grant No. 19-73-10089. TEM analysis was performed by using an equipment at the Joint Research Centre, «Technology and Materials», Belgorod National Research University.

References

[1] F. Abe, T.-U. Kern, R. Viswanathan, Creep-resistant Steels, Woodhead Publishing, Cambridge, 2008.
[2] R.O. Kaybyshev, V.N. Skorobogatykh, I.A. Shchenkova, New martensitic steels for fossil power plant: creep resistance, Phys. Met. Metallogr. 109 (2010) 186–200, https://doi.org/10.1134/S0031918X10020110.
[3] J. Hald, High-alloyed martensitic steel grades for boilers in ultra-supercritical power plants Materials for Ultra-Supercritical and Advanced Ultra-Supercritical Power Plants, in: A. Di Gianfrancesco (Ed.), Materials for Ultra-supercritical and Advanced Ultra-supercritical Power Plant, Woodhead Publishing, Cambridge, 2017, pp. 77–97, https://doi.org/10.1016/B978-0-08-100552-1.00003-8.
[4] I. Nikitin, A. Fedoseeva, R. Kaibyshev, Strengthening mechanisms of creep-resistant 12%Cr-3%Co steel with low N and high B contents, J. Mater. Sci. 55 (2020) 7530–7545, https://doi.org/10.1007/s10853-020-04508-7.
[5] H. Kitahara, R. Ueji, N. Tsuji, Y. Minamino, Crystallographic features of lath martensite in low-carbon steel, Acta Mater. 54 (2006) 1279–1288, https://doi.org/10.1016/j.actamat.2005.11.001.
[6] V. Dudko, A. Belyakov, R. Kaibyshev, Evolution of lath substructure and internal stresses in a 9% Cr steel during creep, ISIJ Int. 57 (2017) 540–549, https://doi.org/10.2355/isijinternational.ISIJINT-2016-334.
[7] N. Dudova, R. Mishnev, R. Kaibyshev, Creep behavior of a 10%Cr heat-resistant martensitic steel with low nitrogen and high boron contents at 650 °C, Mater. Sci. Eng. 766 (2019) 138353, https://doi.org/10.1016/j.msea.2019.138353.
[8] M. Mitsuhara, S. Yamasaki, M. Miake, H. Nakashima, M. Nishida, J. Kusumoto, A. Kanaya, Creep strengthening by lath boundaries in 9Cr ferritic heat-resistant steel, Phil. Mag. Lett. 96 (2016) 76–83, https://doi.org/10.1080/09500839.2016.1154200.
[9] F. Abe, Precipitate design for creep strengthening of 9%Cr tempered martensitic steel for ultra-supercritical power plants, Sci. Technol. Adv. Mater. 9 (2008), 013002, https://doi.org/10.1088/1468-6996/9/1/013002.
[10] R. Mishnev, N. Dudova, A. Fedoseeva, R. Kaibyshev, Microstructural aspects of superior creep resistance of a 10%Cr martensitic steel, Mater. Sci. Eng., A 678 (2016) 178–189, https://doi.org/10.1016/j.msea.2016.09.096.
[11] A. Fedoseeva, N. Dudova, R. Kaibyshev, Creep behavior and microstructure of a 9Cr-3Co-3W martensitic steel, J. Mater. Sci. 52 (2016) 2974–2988, https://doi.org/10.1007/s10853-016-0595-z.
[12] A. Fedoseeva, I. Nikitin, E. Tkachev, R. Mishnev, N. Dudova, R. Kaibyshev, Effect of alloying on the nucleation and growth of Laves phase in the 9–10%Cr-3%Co martensitic steels during creep, Metals 11 (2021) 60, https://doi.org/10.3390/met11010060.
[13] M. Yoshizawa, M. Igarashi, K. Moriguchi, A. Iseda, H.G. Armaki, K. Maruyama, Effect of precipitates on long-term creep deformation properties of P92 and P122 type advanced ferritic steels for USC power plants, Mater. Sci. Eng., A (2009) 162–168, https://doi.org/10.1016/j.msea.2008.05.055, 510–511.
[14] H.G. Armaki, R.P. Chen, K. Maruyama, M. Igarashi, Contribution of recovery mechanisms of microstructure during long-term creep of Gr.91 steels, J. Nucl. Mater. 433 (2013) 23–29, https://doi.org/10.1016/j.jnucmat.2012.09.026.
[15] A. Kostka, K.-G. Tak, R.J. Hellmig, Y. Estrin, G. Eggeler, On the contribution of carbides and micrograin boundaries to the creep strength of tempered martensite ferritic steels, Acta Mater. 55 (2007) 539–550, https://doi.org/10.1016/j.actamat.2006.08.046.
[16] R. Kaibyshev, R. Mishnev, A. Fedoseeva, N. Dudova, The role of microstructure in creep strength of 9-12%Cr steels, Mater. Sci. Forum 879 (2016) 36–41. www.scientific.net/MSF.879.36R.
[17] N. Dudova, A. Plotnikova, D. Molodov, A. Belyakov, R. Kaibyshev, Structural changes of tempered martensitic 9%Cr–2%W–3%Co steel during creep at 650 °C,

Mater. Sci. Eng., A 534 (2012) 632–639, https://doi.org/10.1016/j.msea.2011.12.020.
[18] V. Dudko, A. Belyakov, D. Molodov, R. Kaibyshev, Microstructure evolution and pinning of boundaries by precipitates in a 9pctCr heat resistant steel during creep, Metall. Mater. Trans. 44 (2013) 162–172, https://doi.org/10.1007/s11661-011-0899-1.
[19] A. Fedoseeva, N. Dudova, R. Kaibyshev, Creep strength breakdown and microstructure evolution in a 3%Co modified P92 steel, Mater. Sci. Eng., A 654 (2016) 1–12, https://doi.org/10.1016/j.msea.2015.12.027.
[20] A. Fedoseeva, N. Dudova, R. Kaibyshev, A. Belyakov, Effect of tungsten on creep behavior of 9%Cr–3%Co martensitic steels, Metals 7 (2017) 573, https://doi.org/10.3390/met7120573.
[21] A. Fedoseeva, I. Nikitin, N. Dudova, R. Kaibyshev, Strain-induced Z-phase formation in a 9% Cr-3% Co martensitic steel during creep at elevated temperature, Mater. Sci. Eng., A 724 (2018) 29–36, https://doi.org/10.1016/j.msea.2018.03.081.
[22] F. Abe, T. Ohba, H. Miyazaki, Y. Toda, M. Tabuchi, Effect of W-Mo balance on long-term creep life of 9Cr steel, Mater. A. T. High. Temp. 36 (2019) 314–324, https://doi.org/10.1080/09603409.2018.1555202.
[23] F. Abe, T. Ohba, H. Miyazaki, Y. Toda, M. Tabuchi, Effect of W-Mo balance and boron content on creep rupture ductility of 9Cr steel, Mater. A. T. High. Temp. 36 (2019) 368–378, https://doi.org/10.1080/09603409.2019.1574369.
[24] Y. Liu, S. Tsukamoto, K. Sawada, M. Tabuchi, F. Abe, Precipitation behaviour in Ac3 HAZ simulated B steel during PWHT and creep deformation, Metall. Mater. Trans. 46 (2015) 1843–1854, https://doi.org/10.1007/s11661-015-2802-y.
[25] E. Tkachev, A. Belyakov, R. Kaibyshev, Creep behavior and microstructural evolution of a 9%Cr steel with high B and low N contents, Mater. Sci. Eng., A 725 (2018) 228–241, https://doi.org/10.1016/j.msea.2018.04.032.
[26] A. Fedoseeva, I. Nikitin, N. Dudova, R. Kaibyshev, Superior creep resistance of a high-Cr steel with Re additives, Mater. Lett. 262 (2020) 127183, https://doi.org/10.1016/j.matlet.2019.127183.
[27] A. Fedoseeva, I. Nikitin, N. Dudova, R. Kaibyshev, On effect of rhenium on mechanical properties of a high-Cr creep resistant steel, Mater. Lett. 269 (2019) 81–84, https://doi.org/10.1016/j.matlet.2018.10.081.
[28] J. Vanaja, K. Laha, M.D. Mathew, Effect of tungsten on primary creep deformation and minimum creep rate of reduced activation ferritic-martensitic steel, Metall. Mater. Trans. A Phys. Metall. Mater. Sci. 45 (2014) 5076–5084, https://doi.org/10.1007/s11661-014-2472-1.
[29] J. Vanaja, K. Laha, Assessment of tungsten content on tertiary creep deformation behavior of reduced activation ferritic–martensitic steel, Metall. Mater. Trans. A Phys. Metall. Mater. Sci. 46 (2015) 4669–4679, https://doi.org/10.1007/s11661-015-3075-1.
[30] F. Abe, Creep behavior, deformation mechanisms and creep life of Mod.9Cr-1Mo steel, Metall. Mater. Trans. 46 (2015) 5610–5625, https://doi.org/10.1007/s11661-015-3144-5.
[31] A. Fedoseeva, I. Nikitin, N. Dudova, R. Kaibyshev, Nucleation of W-rich carbides and Laves phase in a Re-containing 10% Cr steel during creep at 650°C, Mater. Char. 169 (2020) 110651, https://doi.org/10.1016/j.matchar.2020.110651.
[32] A. Kipelova, A. Belyakov, R. Kaibyshev, Laves phase evolution in a modified P911 heat resistant steel during creep at 923K, Mater. Sci. Eng., A 532 (2012) 71–77, https://doi.org/10.1016/j.msea.2011.10.064.
[33] G. Dimmler, P. Weinert, E. Kozeschnik, H. Cerjak, Quantification of the Laves phase in advanced 9–12% Cr steels using a standard SEM, Mater. Char. 51 (2003) 341–352, https://doi.org/10.1016/j.matchar.2004.02.003.
[34] D.B. Williams, B.C. Carter, Transmission Electron Microscopy, second ed., Springer, New York, 2009.
[35] A. Fedoseeva, E. Tkachev, V. Dudko, N. Dudova, R. Kaibyshev, Effect of alloying on interfacial energy of precipitation/matrix in high-chromium martensitic steels, J. Mater. Sci. 52 (2017) 4197–4209, https://doi.org/10.1007/s10853-016-0654-5.
[36] A. Fedoseeva, I. Nikitin, N. Dudova, R. Kaibyshev, Effect of normalizing and tempering on structure and mechanical properties of advanced martensitic 10% Cr–3% Co–0.2% Re steel, AIP Conf. Proc. 1909 (2017), 020049, https://doi.org/10.1063/1.5013730.
[37] M.I. Isik, A. Kostka, G. Eggeler, The nucleation of Laves phase particles during high-temperature exposure and creep of tempered martensite ferritic steels, Acta Mater. 81 (2014) 230–240, https://doi.org/10.1016/j.actamat.2014.08.008.
[38] M.I. Isik, A. Kostka, V.A. Yardley, K.G. Pradeep, M.J. Duarte, P.P. Choi, D. Raabe, G. Eggeler, The nucleation of Mo-rich Laves phase particles adjacent to M23C6 micrograin boundary carbides in 12% Cr tempered martensite ferritic steels, Acta Mater. 90 (2015) 94–104, https://doi.org/10.1016/j.actamat.2015.01.027.
[39] I. Fedorova, A. Belyakov, P. Kozlov, V. Skorobogatykh, I. Shenkova, R. Kaibyshev, Laves phase precipitates in a low-carbon 9%Cr martensitic steel during ageing and creep at 923K, Mater. Sci. Eng., A 615 (2014) 153–163, https://doi.org/10.1016/j.msea.2014.07.046.
[40] M. Hättestrand, H.-O. Andrén, Influence of strain on precipitation reactions during creep of an advanced 9% chromium steel, Acta Mater. 49 (2001) 2123–2128, https://doi.org/10.1016/S1359-6454(01)00135-5.
[41] L. Korcakova, J. Hald, A.J. Somers Marcel, Quantification of Laves phase particle size in 9CrW steel, Mater. Char. 47 (2001) 111–117, https://doi.org/10.1016/S1044-5803(01)00159-0.
[42] Y. Xu, Y. Nie, M. Wang, W. Li, X. Jin, The effect of microstructure evolution on the mechanical properties of martensite ferritic steel during long-term aging, Acta Mater. 131 (2017) 110–122, https://doi.org/10.1016/j.actamat.2017.03.045.
[43] Q. Li, Precipitation of Fe_2W Laves phase and modeling of its direct influence on the strength of a 12Cr-2W steel, Metall. Mater. Trans. 37 (2006) 89–97, https://doi.org/10.1007/s11661-006-0155-2.
[44] N. Dudova, R. Kaibyshev, On the precipitation sequence in a 10%Cr steel under tempering, ISIJ Int. 51 (2011) 826–831, https://doi.org/10.2355/isijinternational.51.826.
[45] J.W. Christian, The Theory of Transformation in Metals and Alloys, Pergamon Press, Oxford, 2002.
[46] E.J. Mittemeijer, Fundamentals of Materials Science: the Microstructure–Property Relationship Using Metals as Model Systems, Chap. 9, Springer Verlag, New York, 2010. Phase Transformations.
[47] F. Liu, F. Sommer, C. Bos, E.J. Mittemeijer, Analysis of solid state phase transformation kinetics: models and recipes, Int. Mater. Rev. 52 (2007) 193–212, https://doi.org/10.1179/174328007X160308.
[48] M.P. Sello, W.E. Stumpf, Laves phase precipitation and its transformation kinetics in the ferritic stainless steel type AISI 441, Mater. Sci. Eng., A 528 (2011) 1840–1847, https://doi.org/10.1016/j.msea.2010.09.090.
[49] O. Prat, J. Garcia, D. Rojas, C. Carrasco, G. Inden, Investigations on the growth kinetics of Laves phase precipitates in 12%Cr creep-resistant steels: experimental and DICTRA calculations, Acta Mater. 58 (2010) 6142–6153, https://doi.org/10.1016/j.actamat.2010.07.033.
[50] O. Prat, J. Garcia, D. Rojas, G. Sauthoff, G. Inden, The role of Laves phase on microstructure evolution and creep strength of novel 9%Cr heat resistant steels, Intermetallics 32 (2013) 362–372, https://doi.org/10.1016/j.intermet.2012.08.016.
[51] L. Maddi, G.S. Deshmukh, A.R. Ballal, D.R. Peshwe, R.K. Paretkar, K. Laha, M. D. Mathew, Effect of Laves phase on the creep rupture properties of P92 steel, Mater. Sci. Eng., A 668 (2016) 215–223, https://doi.org/10.1016/j.msea.2016.05.074.
[52] K. Miyata, Y. Sawaragi, Effect of Mo and W on the phase stability of precipitates in low Cr heat resistant steels, ISIJ Int. 41 (2001) 281–289, https://doi.org/10.2355/isijinternational.41.281.
[53] Sh Qiao, Y. Wei, H. Xu, H. Cui, F. Lu, The evolution behavior of second phases during long-term creep rupture process for modified 9Cr-1.5Mo-1Co steel welded joint, Mater. Char. 151 (2019) 318–331, https://doi.org/10.1016/j.matchar.2019.03.020.
[54] X. Wang, Q. Xu, Sh Yu, H. Liu, L. Hu, Y. Ren, Laves-phase evolution during aging in fine grained heat-affected zone of a tungsten-strengthened 9% Cr steel weldment, J. Mater. Process. Technol. 219 (2015) 60–69, https://doi.org/10.1016/j.jmatprotec.2014.12.007.
[55] X. Wang, Q. Xu, S. Yu, L. Hu, H. Liu, Y. Ren, Laves-phase evolution during aging in 9Cr-1.8W-0.5Mo-VNb steel for USC power plants, Mater. Chem. Phys. 163 (2015) 219–228, https://doi.org/10.1016/j.matchemphys.2015.07.032.
[56] A.Yu Kipelova, A.N. Belyakov, V.N. Skorobogatykh, I.A. Shchenkova, R. O. Kaibyshev, Tempering-induced structural changes in steel 10Kh9K3V1M1FBR and their effect on the mechanical properties, Met. Sci. Heat Treat. 52 (2010) 100–110, https://doi.org/10.1007/s11041-010-9240-7.
[57] J. Cermak, J. Ruzickova, A. Pokorna, Grain boundary diffusion of 181W in Fe-Cr ferritic alloys, Scripta Metall. Mater. 33 (1995) 289–294, https://doi.org/10.1016/0956-716X(95)00160-W.
[58] S. Takemoto, H. Nitta, Y. Iijima, Y. Yamazaki, Diffusion of tungsten in α-iron, Phil. Mag. 87 (2007) 1619–1629, https://doi.org/10.1080/14786430600732093.
[59] R.A. Pérez, D.N. Torres, W diffusion in paramagnetic and ferromagnetic α-Fe, Appl. Phys. A 104 (2011) 329–333, https://doi.org/10.1007/s00339-010-6142-x.
[60] Sh Huang, D.L. Worthington, M. Asta, V. Ozolins, G. Ghosh, P.K. Lia, Calculation of impurity diffusivities in a-Fe using first-principles methods, Acta Mater. 58 (2010), https://doi.org/10.1016/j.actamat.2009.11.041, 1982–1993.
[61] R. Wagner, R. Kampmann, Homogeneous second phase precipitation, in: P. Haasen (Ed.), Phase Transformations in Materials, Materials Science Monographs, John Wiley & Sons Inc., New York, 1991, pp. 213–303.
[62] I.M. Lifshitz, V.V. Slyozov, The kinetics of precipitation from supersaturated solid solutions, J. Phys. Chem. Solid. 19 (1961) 35–50, https://doi.org/10.1016/0022-3697(61)90054-3.
[63] F. Abe, Coarsening behavior of lath and its effect on creep rates in tempered martensitic 9Cr–W steels, Mater. Sci. Eng., A 387–389 (2004) 565–569, https://doi.org/10.1016/j.msea.2004.01.057.
[64] A.J. Ardell, On the coarsening of grain boundary precipitates, Acta Metall. 20 (1972) 601–609, https://doi.org/10.1016/0001-6160(72)90015-6.
[65] H.O.K. Kirchner, Coarsening of grain-boundary precipitates, Metall. Trans. 2 (1972) 2861–2864, https://doi.org/10.1007/BF02813264.
[66] A. Fedoseeva, N. Dudova, R. Kaibyshev, Effect of stresses on the structural changes in high-chromium steel upon creep, Phys. Met. Metallogr. 118 (2017) 591–600, https://doi.org/10.1134/S0031918X17040032.
[67] L. Morsdorf, O. Jeannin, D. Barbier, M. Mitsuhara, D. Raabe, C.C. Tasan, Multiple mechanisms of lath martensite plasticity, Acta Mater. 121 (2016) 202–214, https://doi.org/10.1016/j.actamat.2016.09.006.
[68] C.C. Kinney, K.R. Pytlewski, A.G. Khachaturyan, J.W. Morris Jr., The microstructure of lath martensite in quenched 9Ni steel, Acta Mater. 69 (2014) 372–385, https://doi.org/10.1016/j.actamat.2014.01.058.
[69] J. Inoue, A. Sadeghi, T. Koseki, Slip band formation at free surface of lath martensite in low carbon steel, Acta Mater. 165 (2019) 129–141, https://doi.org/10.1016/j.actamat.2018.11.026.

[70] H. Na, Sh Nambu, M. Ojima, J. Inoue, T. Koseki, Crystallographic and microstructural studies of lath martensitic steel during tensile deformation, Metall. Mater. Trans. 45 (2014) 5029–5043, https://doi.org/10.1007/s11661-014-2461-4.
[71] F. Abe, Effect of fine precipitation and subsequent coarsening of Fe_2W Laves phase on the creep deformation behavior of tempered martensitic 9Cr-W steels, Metall. Trans. A 36A (2005) 321–332, https://doi.org/10.1007/s11661-005-0305-y.
[72] R. Kaibyshev, F. Musin, E. Avtokratova, Y. Motohashi, Deformation behavior of a modified 5083 aluminum alloy, Mater. Sci. Eng., A 392 (2005) 373–379, https://doi.org/10.1016/j.msea.2004.10.002.